Atmospheric Environment 45 (2011) 5025–5032

Contents lists available at ScienceDirect

Atmospheric Environment

journal homepage: www.elsevier.com/locate/atmosenv

A photochemical source of peroxypropionic and peroxyisobutanoic nitric anhydride

Amanda Furgeson, Levi H. Mielke, Dipayan Paul, Hans D. Osthoff*

Department of Chemistry, University of Calgary, 2500 University Drive NW, Calgary, AB T2N 1N4, Canada

ARTICLE INFO

Article history:
Received 2 August 2010
Received in revised form
28 March 2011
Accepted 29 March 2011

Keywords:
Peroxycarboxylic nitric anhydrides (PAN)
Peroxypropionic nitric anhydride (PPN)
Peroxyisobutanoic nitric anhydride (PiBN)
In situ photolysis source
Thermal dissociation chemical ionization mass spectrometry (TD-CIMS)
Thermal dissociation cavity ring-down spectroscopy (TD-CRDS)
Calibration

ABSTRACT

A method to photochemically generate stable outputs of peroxyacetic, peroxypropionic, or peroxyisobutanoic nitric anhydride (PAN, PPN, or PiBN) in dilute gas streams is described. The PANs are generated by photolysis of excess acetone, diethyl ketone, or diisopropyl ketone in the presence of oxygen and either nitric oxide or nitrogen dioxide. The source output was characterized using a commercial NO_y monitor, an in-house constructed thermal dissociation cavity ring-down spectrometer (TD-CRDS) equipped with a heated inlet for quantification of NO_2, total peroxyacyl nitrates ($\sum$PAN), and total alkyl nitrates ($\sum$AN), and a thermal dissociation chemical ionization mass spectrometer (TD-CIMS) operated with iodide reagent ion. The TD-CIMS was calibrated (against TD-CRDS) using diffusion sources containing synthetic PAN standards. Response factors of 21, 19, and 5 counts per pptv, normalized to 1 million counts of iodide reagent ion, were found for PAN (monitored at *m/z* 59), PPN (*m/z* 73), and PiBN (*m/z* 87), respectively. The photo source was found to generate the three PANs in high yield. CIMS response factors derived using the photo source and TD-CRDS were identical to those derived from synthetic standards for PAN and PPN; hence, the photochemical PAN and PPN sources may be used to calibrate TD-CIMS (against TD-CRDS). For PiBN, the response factor derived using the photo source was 60% larger than that derived using the synthetic standard, limiting its use to deliver a calibrated stream of PiBN.

1. Introduction

Peroxycarboxylic nitric anhydrides (PANs), usually known by their non-IUPAC name peroxyacyl nitrates, are important trace gas constituents of the troposphere (Roberts, 1990, 2007). More than 43 different PANs are known; in ambient air, peroxyacetic nitric anhydride (PAN, $CH_3C(O)O_2NO_2$), commonly referred to as peroxyacetyl nitrate, is usually the most abundant PAN species and often also the most abundant odd nitrogen, or NO_y ($\equiv$ NO + NO_2 + $\sum$PAN + $\sum$AN + HNO_3 + HONO + NO_3 + 2 N_2O_5 + $ClNO_2$ + …) species. PANs are formed as byproducts in the same photochemistry between NO_x ($\equiv$ NO + NO_2) and volatile organic compounds (VOCs) that produces ozone (O_3); they are thus good chemical markers to study the O_3-formation process (Roberts, 2007).

Over the years, a variety of techniques to quantify mixing ratios of PANs in ambient air have been developed. A widely used and mature technique is gas chromatography with electron capture detection, or GC–ECD (e.g., Darley et al., 1963; Schrimpf et al., 1995; Williams et al., 2000; Volz-Thomas et al., 2002; Flocke et al., 2005). A relatively new but increasingly popular technique is thermal dissociation chemical ionization mass spectrometry (TD-CIMS). In this technique, the PANs are dissociated in a heated inlet, and the generated peroxyacyl radicals are converted to, and detected as, the carboxylate anions using I^- as the reagent ion (Slusher et al., 2004). The TD-CIMS requires continuous addition of an isotopically labeled internal standard because the instrument response is matrix-dependent (Slusher et al., 2004). Both PAN measurement techniques require calibration; the GC–ECD in particular needs to be calibrated for each PAN monitored as its response factor is different for each PAN (Flocke et al., 2005). The TD-CIMS is known to exhibit similar response factors for PAN and peroxypropionic nitric anhydride ($C_2H_5C(O)O_2NO_2$, PPN); the response factor for peroxyisobutanoic nitric anhydride ($CH_3CH(CH_3)C(O)O_2NO_2$, PiBN) was estimated to be of similar magnitude as that of PAN and PPN by Slusher et al. (2004), but was very recently found to be an order of magnitude lower for PiBN than for PAN or PPN (Zheng et al., 2011).

Diffusion sources, calibrated against NO_y chemiluminescence (CL) instruments, are commonly used to determine the response factors of PAN instruments. The use of diffusion sources requires

* Corresponding author. Tel.: +1 403 220 8689; fax: +1 403 289 9488.
E-mail address: hosthoff@ucalgary.ca (H.D. Osthoff).

1352-2310/$ – see front matter © 2011 Elsevier Ltd. All rights reserved.
doi:10.1016/j.atmosenv.2011.03.072

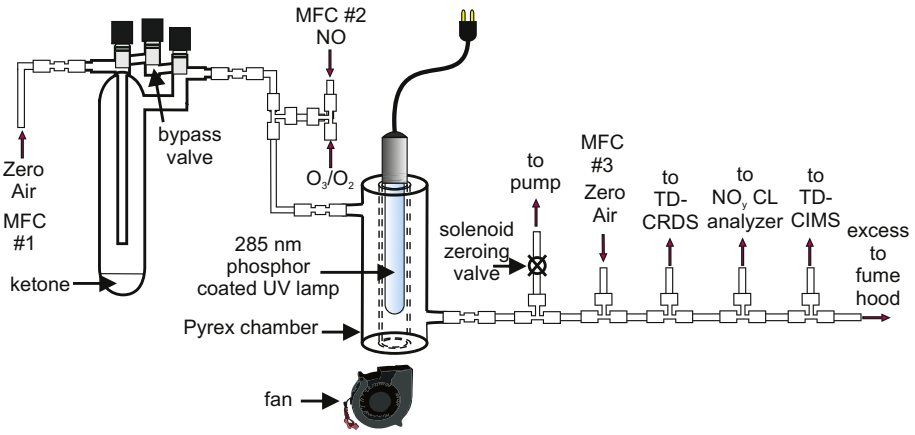

Fig. 1. Schematic diagram of photolysis source setup. MFC = mass flow controller. For a detailed description, see Section 2.1 in the text.

laborious and non-trivial syntheses of PAN standards in high purity and storage of these in a non-polar solvent (e.g., tridecane) at cold temperatures, e.g., in an ice-water bath. This is necessary since PANs are explosive and are prone to thermal decomposition. Often, the use of a preparative-scale GC to separate PAN from other forms of NO_y becomes necessary (Flocke et al., 2005).

An alternative method to calibrate PAN instruments is to generate PAN species in situ by photochemical means (Grosjean et al., 1984; Warneck and Zerbach, 1992). The photochemical PAN sources are attractive as they usually provide a more stable output than diffusion sources and eliminate the need for laborious syntheses, purification procedures, cold storage, and transport. In the most commonly used method, a mixture of excess acetone in a calibrated gas stream of NO (or NO_2) in the presence of oxygen is irradiated by a UV light source to produce PAN in nearly quantitative yield (Warneck and Zerbach, 1992; Emrich and Warneck, 2000; Pätz et al., 2002; Volz-Thomas et al., 2002; Flocke et al., 2005). To date, there has been only one report in the open literature extending the ketone photolysis method to PAN species other than PAN. Volz-Thomas et al. (2002) reported that photolysis of 3-pentanone (diethyl ketone) with a mercury pen ray lamp in the presence of NO and O_2 yielded an approximately equimolar mixture of PPN and ethyl nitrate. They concluded that 3-pentanone was not a useful precursor to generate accurate PPN calibration gases as the major impurity, ethyl nitrate, would interfere with calibration against NO_y CL instruments.

In this paper, a method to generate peroxycarboxylic nitric anhydrides by dialkyl ketone photolysis is described. PAN, PPN or PiBN were generated in high yields by photolysis of either acetone, 3-pentanone or 2,4-dimethyl-3-pentanone in the presence of NO (or NO_2) and oxygen. PAN yields were increased by using a phosphor-coated Hg pen ray lamp (Flocke et al., 2005) and a Pyrex photo reactor instead of one made of quartz. The output from the source was monitored using a thermal dissociation cavity ring-down spectrometer (TD-CRDS) capable of distinguishing between and quantifying mixing ratios of NO_2, total peroxyacyl nitrate ($\sum$PAN), and total alkyl nitrate ($\sum$AN) (Paul et al., 2009; Paul and Osthoff, 2010). The output of the photo source was used to determine the response factors of a TD-CIMS, previously calibrated using diffusion sources containing synthetic standards, against TD-CRDS. Advantages and limitations of calibrating a TD-CIMS using photochemically generated samples of PAN, PPN or PiBN are discussed.

2. Experimental section

2.1. Setup and operation of the photolysis source

A schematic setup of the photolysis source is shown in Fig. 1. Connecting tubing was constructed from PFA Teflon. The liquid ketone of interest (Table 1; used as received from Sigma–Aldrich) was placed in a glass reservoir, and the head space was flushed with ultrapure, or "zero", air (Praxair) at typical flow rates of 20–100 standard-cubic-centimeters per minute (sccm) with the aid of a calibrated mass flow controller (MFC #1; range 0–500 sccm). At a 100 sccm flow rate, the mixing ratio of acetone delivered was approximately 940 parts-per-million by volume (10^{-6}, ppmv), measured off-line by FTIR using a Bruker Tensor 27 equipped with a Gemini Venus multi-pass gas cell with 6.4 m optical path length. Infrared absorption cross-sections were obtained from the Pacific Northwest National Laboratory's vapor phase infrared spectral library. The other ketones used (Table 1) have somewhat lower vapor pressures than acetone; their concentrations in the gas streams were accordingly lower. For example, 3-pentanone yielded a mixing ratio of approximately 120 ppmv under the same experimental conditions as the acetone quantification.

Up to 35 sccm of nitric oxide (Praxair, 2.28 ppmv (±5%) in N_2) were added to the ketone diffusion source effluent via a sidearm by means of a second mass flow controller (MFC #2, range 100 sccm). In some of the experiments, NO was oxidized to NO_2 prior to entering the main photolysis chamber using a stoichiometric amount of O_3 generated by passing a stream of O_2 (flow rate set to 76 sccm using a 50 μm critical orifice and 55 psi back pressure) past a 254 nm Hg lamp with variable exposure length (VWR). Alternatively, up to 1 sccm of nitrogen dioxide (Praxair, 120 ppmv in zero air) using a 20 sccm all-metal MFC were added. Under these

Table 1
Overview of PAN species generated by photolysis in this work.

Name of ketone	Grade (Purity)	Formula	V.P. (mm Hg)	PAN species generated	Acronym
Acetone	Chromasolv Plus > 99.9%	$CH_3C(O)CH_3$	184	$CH_3C(O)O_2NO_2$	PAN
3-Pentanone (diethyl ketone)	Reagentplus > 99%	$C_2H_5C(O)C_2H_5$	28	$C_2H_5C(O)O_2NO_2$	PPN
2,4-Dimethyl-3-pentanone (diisopropyl ketone)	98%	$(CH_3)_2CHC(O)CH(CH_3)_2$	3.7	$(CH_3)_2CHC(O)O_2NO_2$	PiBN

V.P. = room temperature vapor pressure taken from material safety data sheets (MSDS).

conditions, the mixing ratio in the gas mixture entering the photolysis chamber ranged up to 600 parts-per-billion (10^{-9}, ppbv) of NO, or up to 1200 ppbv of NO_2.

The ketones were photodissociated using a 2-inch long phosphor-coated Hg pen ray UV lamp (Jelight, model 84-285-2). The UV lamp was placed axially inside a specially constructed cylindrical photolysis chamber (internal volume 75 mL; minimum residence time = 45 s) and was physically separated from the sample gas by the 2 mm thick glass chamber wall. Two different cells were constructed and tested: The first was made from fused silica (quartz) and the other was made from Pyrex. The UV lamp was cooled using a high-velocity fan (EBM Pabst Flatpak blower RG90-18/06) placed axially to the photolysis cell. The temperature of the gas stream exiting the photolysis chamber was measured by inserting a thermocouple into a tee directly beyond the exit of the chamber. The temperature remained at room temperature even after the lamp had been operated for approximately 1 h.

The photolysis chamber effluent was further diluted with up to 19.5 standard-liters-per-minute (slpm) of zero air with the aid of a third mass flow controller (MFC #3, range 0–30 slpm) before being analyzed in parallel by the TD-CIMS, TD-CRDS and NO_y CL analyzer. Excess flow was vented. The dilution step (up to 1:200) provided sufficient sample volume for all instruments during both sampling and zeroing modes. It limited the concentration of PAN that could be measured by all instruments in parallel to a maximum of about 5 ppbv. For zeroing, the flow exiting the photolysis chamber was diverted with a solenoid valve connected to a vacuum pump.

2.2. Thermal dissociation cavity ring-down spectroscopy

Mixing ratios of NO_2, $\sum$PAN and $\sum$AN emitted from the photolysis source were quantified by TD-CRDS. In initial experiments, the 532 nm Nd:YAG TD-CRDS described by Paul et al. (2009) was used. Since these experiments were conducted under non-ideal laboratory temperature conditions (frequently exceeding 30 °C due to a central air conditioning failure), some of the experiments were repeated in January and February 2010, and again in January and February 2011, using the 405 nm blue diode laser TD-CRDS described by Paul and Osthoff (2010). Both instruments had two sample cells: The first served as a reference, quantifying background NO_2 mixing ratios at room temperature. The second inlet was heated and operated at either 250 °C (to dissociate $\sum$PAN to NO_2) or 450 °C (to dissociate $\sum$PAN and $\sum$AN to NO_2). The peroxy and alkyl nitrates were then quantified by difference. Because the output of the photolysis source contained high levels of ketones in some of the experiments, the ring-down time constants of the "empty" cavities, t_0, were determined under flow with the ketone source inline but without adding NO or engaging the UV lamp.

2.3. Chemiluminescence measurements

Mixing ratios of NO and NO_y were monitored using a commercial NO_y CL analyzer (Thermo Scientific, Model 42i). This instrument utilizes a molybdenum converter heated to 325 °C to convert the various NO_y species to NO; an automated valve allows bypassing of the Mo converter and enables alternating measurements of NO and NO_y. The response to NO was calibrated using the dilution factors of factory-calibrated MFCs and an NO cylinder of certified concentration. Since delivery from NO_2 gas cylinders can be unreliable, the NO_y conversion efficiency was calibrated as follows: Dilute gas streams containing NO_2 were sampled simultaneously by TD-CRDS and the CL analyzer, and the response of the NO_y instrument (i.e., slope) was scaled to that of the TD-CRDS.

2.4. Thermal dissociation chemical ionization mass spectrometry

The output of the photo source and TD-CRDS were used to calibrate a commercial TD-CIMS (THS instruments), which also served to verify the identity of the $\sum$PAN species generated in the photochemical source. The instrument is similar to the one described by Slusher et al. (2004) and will be described in more detail in a forthcoming publication. Briefly, a Teflon inlet heated to 180 °C was used to dissociate the PANs in the sample stream, producing RC(O)OO· radicals and NO_2. Upon entering the ionization region (operated at 19 torr), the peroxyacyl radicals were reacted with I^- reagent ion (generated by passing methyl iodide past a ^{210}Po α-particle emitter) to generate carboxylate ($RC(O)O^-$) anions. Deliberate addition of excess NO (which titrates the peroxyacyl radicals) was used to determine the background counts at each of the PAN masses. Since the yield of the carboxylate anions is highest in a humidified buffer gas (Slusher et al., 2004), the inlet flow was diluted with a humidified stream of nitrogen to yield a sample with approximately 14% relative humidity. A collisional dissociation chamber (CDC) was used to break up water clusters. Ions are selected using a quadrupole mass analyzer and counted using a channeltron detector. Mass counts were normalized to 1,000,000 counts of I^- before presentation. Response (calibration) factors were obtained from simultaneous measurements by TD-CRDS of the output passive diffusion sources containing PAN samples (synthesized as described below) and compared to response factors obtained with the aid of the photo source.

2.5. Synthesis of PAN standards and setup and operation of passive diffusion source

PAN, PPN, and PiBN were synthesized from the corresponding peroxycarboxylic acid, generated by reaction of H_2O_2 with acetic, propionic, or isobutanoic acid anhydride, respectively. The peroxycarboxylic acid was then reacted with HNO_3 in the presence of H_2SO_4 and tridecane at 0 °C following a procedure by J. Roberts (personal communication) which is based on the method by Nielsen and Gaffney (Nielsen et al., 1982; Gaffney et al., 1984). The solutions were stored in small batches (in tridecane) in the freezer until use. The synthetic standards were placed in a glass reservoir and the head space was flushed with nitrogen (Praxair) at a flow rate of 82 sccm. This was done with the use of a 50 μm critical orifice and a back pressure of 60 psi delivered by a nitrogen cylinder. The gas stream exiting the glass reservoir was diluted with zero air using a 0–30 slpm mass flow controller. Excess flow was vented. The resulting output of the passive diffusion source was sampled simultaneously by all instruments. The passive diffusion source effluent purity was verified for PAN by FTIR to be >94% (relative to NO_y species), with HNO_3 as the major impurity.

3. Results

3.1. Comparison of quartz and Pyrex photolysis chambers

Fig. 2 shows the emission spectra of the phosphor-coated lamp, recorded with a miniature spectrometer (Ocean Optics USB-2000), and the absorption spectra of the ketones used in this work. The blue trace shows the emission spectrum observed through quartz which contains considerable intensity at 254 nm. The red trace shows the emission spectrum of the lamp observed through Pyrex. The 254 nm line is fully suppressed, and the UV light at wavelengths < 325 nm is attenuated. Both emission spectra partially overlap with the absorption spectra of the ketones.

Representative TD-CRDS thermal dissociation profiles of the output of both photo sources are shown in Fig. 3. The red data

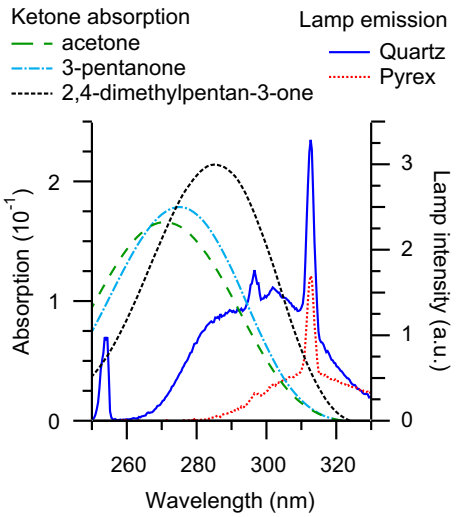

Fig. 2. Overlap of the (n, π^*) band of selected dialkyl ketones (left axis) with the lamp emission spectra, observed through either quartz (**blue solid trace, right axis**) or Pyrex (**red dashed trace**). The ketone spectra were recorded on a Varian "Cary 5000" UV–Vis spectrometer. Samples were prepared in a 1.0 cm cuvette, and approximately 20 mL of the ketone were dissolved in 5 mL methanol. (For interpretation of the references to colour in this figure legend, the reader is referred to the web version of this article.)

points show the thermal dissociation profile of the output from the Pyrex cell photo source. The maximum amount of NO_2 is observed at an inlet temperature of 200 °C, which indicates that the source output contained PAN only. The blue data points show the results obtained with the quartz cell. In this case, two distinct plateaus are observed. The signal observed in the range from about 190 °C–290 °C corresponds to the amount of PAN present (~70%), and the further increase at inlet temperatures approaching 450 °C is due thermal dissociation of alkyl nitrates (~30%). Thus, the output of the source using the quartz cell contained a mixture of PAN and alkyl nitrates. In the particular case shown, the yield of alkyl nitrates was exceptionally high as the cell was not actively

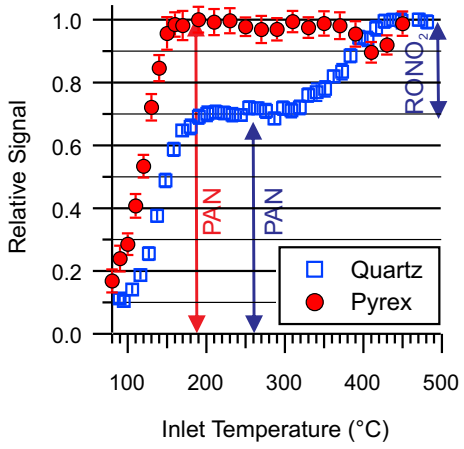

Fig. 3. Thermal dissociation profiles observed by thermal dissociation cavity ring-down spectroscopy. The ordinate indicates the set point temperature of the heated inlet. PAN quantitatively converts to NO_2 above 200 °C. Alkyl nitrates dissociate at temperatures above 300 °C and are fully converted at a temperature of 425 °C **(blue trace)** Thermal dissociation profile observed when a warm quartz chamber was used. The photolysis source emitted a 2:1 mixture of PAN:Methyl nitrate. **(red trace)** Thermal dissociation profile observed when a room temperature (25 °C) Pyrex chamber was used. The output does not contain a measurable amount of alkyl nitrate. (For interpretation of the references to color in this figure legend, the reader is referred to the web version of this article.)

cooled using a fan. However, even when the reaction vessel was cooled, non-negligible quantities of alkyl nitrates were observed by TD-CRDS.

3.2. Photochemical production of PPN and calibration of TD-CIMS

The top panel of Fig. 4 shows a time series of NO_2, ∑PAN and NO_2+∑PAN (quantified by TD-CRDS) emitted from the Pyrex photo source using diethyl ketone and NO, oxidized to NO_2 with O_3 prior to entering the photolysis cell, as reagents. The source was by-passed regularly (shown as the dark gray underlay). The amount of NO reagent (calculated from the flow dilution ratios and shown as a dashed purple trace) was changed periodically. The UV lamp was switched on (shown as a light gray underlay) and off several times. An excess amount of NO (shown with a light yellow underlay), delivered from a cylinder containing 0.1% NO in N_2 via a 50 μm critical orifice (10 psi back pressure), was added periodically to determine the background counts of the TD-CIMS. This "zeroing NO" also contained NO_2; hence, the TD-CRDS signals go off-scale during those periods.

The plot on the left-hand side (lhs) of Fig. 5 shows the amount of ∑PAN (open circles) and NO_2 + ∑PAN observed against the calculated amount of reagent NO gas. The amount of PPN generated scales linearly with the amount of NO added to the photo source, and the source produces PPN in high yield (77%, Table 2). The amount of NO_2+∑PAN observed is (92.9 ± 0.7)% and slightly less than the amount of NO_x added to the source.

The bottom panel of Fig. 4 shows the number of counts observed at m/z 73 (propionate anion, used to quantify PPN) and m/z 59 (acetate anion, used to quantify PAN), normalized to 1,000,000

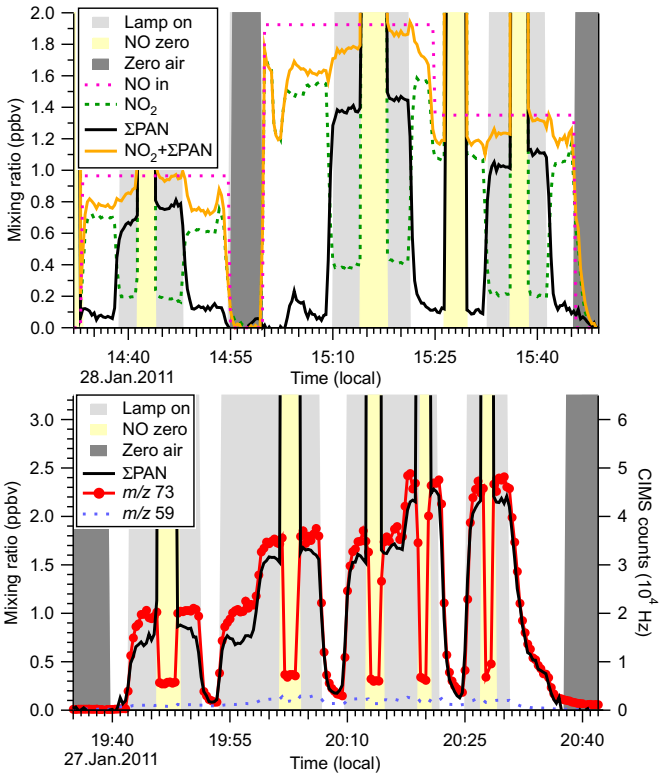

Fig. 4. (Top panel) Production of PPN using the Pyrex photo source and diethyl ketone as reagent. Flow conditions: MFC #1 = 5.0 sccm, MFC #2 = 0–11 sccm (NO in N_2, 2.28 ppmv) diluted with 76 sccm trace O_3 in O_2, MFC #3 = 9.6 slpm. (**bottom panel**). Time series of ∑PAN observed by TD-CRDS (left axis) and m/z 73 and m/z 59 observed by TD-CIMS (right axis).

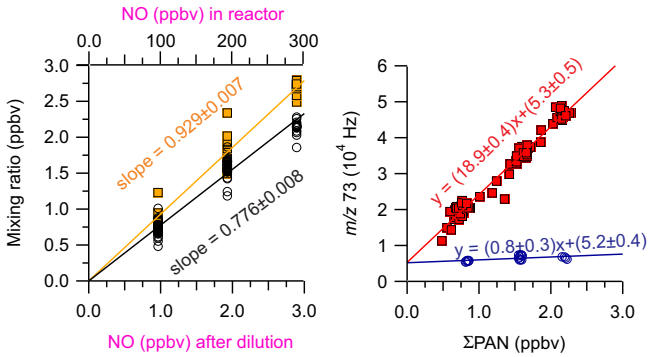

Fig. 5. (Left hand side). Plots of ∑PAN (open circles, black) and NO_2+∑PAN (solid squares, orange) of the data shown in the top panel of Fig. 4 during times when the photolysis lamp was switched on against the calculated amount of NO delivered to the photo source (top axis) and the amount of NO that is delivered prior to switching the lamp on to the instruments (bottom axis). The uncertainties are ±1 σ of linear fits (forced through a zero intercept) and do not include systematic uncertainties (**Right hand side**). Scatter plots of the data shown in the bottom panel of Fig. 4 during times when the photolysis lamp was switched on (solid squares) and when the zeroing NO was added (open circles). (For interpretation of the references to colour in this figure legend, the reader is referred to the web version of this article.)

counts of iodide ion, during the same time period. The major anion observed is *m/z* 73, consistent with the use of diethyl ketone as reagent in the photo source. The TD-CIMS counts at *m/z* 73 are highly correlated ($r^2 = 0.97$) with the TD-CRDS ∑PAN signal; the scatter plot has a slope (or response factor) of (18.9 ± 0.4) counts $pptv^{-1}$ and an offset of (5.3 ± 0.5) × 1000 counts (Fig. 5, right-hand side (rhs), red solid squares). This offset is not strongly dependent on the amount of NO_x added to the photo source and is accurately measured during the NO zeroing periods to (5.2 ± 0.4) × 1000 counts (shown as blue open circles). The response factor derived using the photochemical source was identical to that derived using a synthetic standard placed in a diffusion source.

3.3. Photochemical production of PiBN and calibration of TD-CIMS

Fig. 6 and Fig. 7 show similar plots as Figs. 4 and 5, but with diisopropyl ketone as the reagent and PiBN (monitored at *m/z* 87) as the product. The time series of *m/z* 87, *m/z* 73 and *m/z* 59 shown in the bottom panel of Fig. 6 verify that PiBN is the major PAN photo product emitted by the photo source. Based on the amount of NO_x added to the photo source, PiBN was generated with 75% yield (Table 2) relative to the amount of NO added (Fig. 7, lhs). Similar to what was observed for PPN, the CIMS observes approximately 5000 cts at *m/z* 87 that are not affected by titration with excess NO. The CIMS response factor for PiBN, derived with the output of the photo source, was (8.2 ± 0.2) counts $pptv^{-1}$ ($r^2 = 0.93$; Fig. 7, rhs), higher than the response factor of (4.5 ± 0.1) counts $pptv^{-1}$ derived using a synthetic standard (Table 3).

Table 2
Typical yields of photolysis products relative to the amount of NO_x added to the Pyrex photo source.

Date	Form of NO_x added	Species generated	Yield	r^2	Concentration range (ppbv)
2009	NO	PAN	0.932 ± 0.002	0.995	0–5
2009	NO	PAN + NO_2	0.986 ± 0.004	0.994	0–5
2011	NO_2	PAN	0.775 ± 0.005	0.935	0–2
2011	NO_2	PAN + NO_2	1.000 ± 0.008	0.934	0–2
2009	NO	PPN	0.871 ± 0.004	0.990	0–4
2009	NO	PPN + NO_2	0.901 ± 0.004	0.991	0–4
2010	NO_2[b]	PPN	0.869 ± 0.032	0.987	0–3
2010	NO_2[b]	PPN + NO_2	0.963 ± 0.032	0.987	0–3
2011	NO_2[a]	PPN	0.776 ± 0.008	0.944	0–2.5
2011	NO_2[a]	PPN + NO_2	0.929 ± 0.007	0.969	0–2.5
2009	NO	PiBN	0.736 ± 0.003	0.990	0–4
2009	NO	PiBN + NO_2	0.951 ± 0.004	0.993	0–4
2011	NO_2[c]	PiBN	0.750 ± 0.006	0.960	0–1.5
2011	NO_2[c]	PiBN + NO_2	0.946 ± 0.005	0.975	0–1.5

Yields were determined from linear fits of plots of ∑PAN or ∑PAN + NO_2 observed by TD-CRDS against the (calculated) amount of NO_x added to the photolysis cell with the intercept forced to zero. The uncertainties stated are the ±1 σ precisions of the slopes of the linear fits and do not include uncertainties in the calibration of the amount of NO (or NO_2) delivered.
[a] Data shown in Figs. 4 and 5.
[b] Data shown in Figs. 6 and 7.
[c] Data shown in Fig. 8.

3.4. Direct comparison of calibrations using photochemically generated and synthetic PPN samples

Fig. 8 shows simultaneous measurements of PPN by TD-CRDS (blue trace) and TD-CIMS (red trace). Initially, the output of the Pyrex photochemical source was sampled. For this particular experiment, we chose NO_2 as a reagent and monitored its mixing ratios by TD-CRDS (green trace). The TD-CRDS and TD-CIMS PPN measurements were highly correlated ($r^2 = 0.986$). On/off cycling of the UV lamp demonstrates the photolytic formation of PPN from NO_2. Conversion of NO_2 to PPN in the photo source was high (87%, Table 2). The response factor of the TD-CIMS at *m/z* 73 for the time period shown in Fig. 8 was (13.0 ± 0.1) normalized counts $pptv^{-1}$. The operating conditions of the TD-CIMS (e.g., inlet pressure, activity of ion source, etc.) were different from those in the experiments shown in Figs. 4 and 5, so that the response factors are not directly comparable.

Table 3
Comparison of TD-CIMS response factors normalized to 1,000,000 counts of I^-.

Date	Molecule	Source	Response factor (counts $pptv^{-1}$)	Concentration range (ppbv)
Feb 16, 2011	PAN	Photo	21.5 ± 0.8	0–1.8
Jan 24, 2011	PPN	Diffusion	20.1 ± 0.9	0–1.5
Jan 27, 2011[a]	PPN	Photo	18.9 ± 0.4	0–2.5
Feb 28, 2011	PPN	Diffusion (new sample)	18.8 ± 0.2	0–3
Feb 28, 2011	PPN	Diffusion (aged sample)	17.1 ± 0.1	0–10
Jan 28, 2011[b]	PiBN	Photo	8.2 ± 0.2	0–1.5
Feb 28, 2011	PiBN	Diffusion	4.9 ± 0.1	0–10
Mar 2, 2011	PiBN	Photo	8.2 ± 0.4	0–1.0
Mar 2, 2011	PiBN	Diffusion	4.5 ± 0.1	0–5.0

Data acquired in 2009 and 2010 are not included in this comparison since the operating conditions of the TD-CIMS were not the same.
[a] Data shown in Figs. 4 and 5.
[b] Data shown in Figs. 6 and 7.

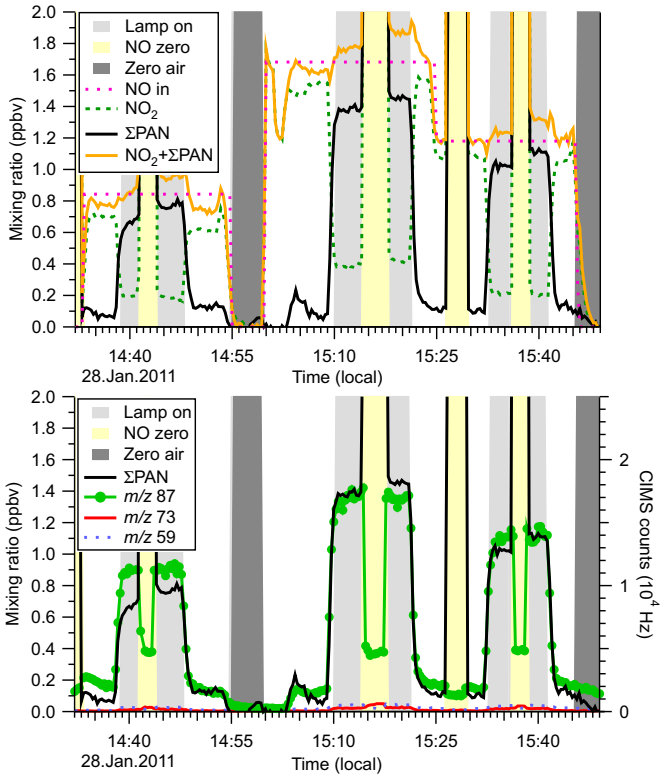

Fig. 6. Production of PiBN using the Pyrex photo source and diisopropyl ketone as reagent. Flow conditions are the same as in Fig. 4.

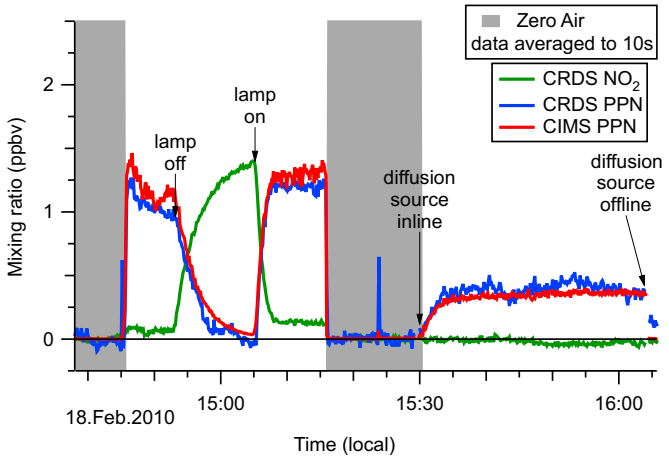

Fig. 8. Verification of TD-CIMS calibration parameters for PPN. The photolysis source (with diethyl ketone) was used until 15:20, and replaced by a diffusion source containing a synthetic PPN standard thereafter. Counts at *m/z* 73 were converted to mixing ratios using a constant response factor of 13 counts $pptv^{-1}$. Flow conditions: MFC #1 = 20 sccm, MFC #2 = 0–0.20 sccm (NO_2 in zero air, 120 ppmv), MFC #3 = 7.8 slpm. Between 15:11 and 15:14, the TD-CRDS inlet temperature was briefly increased to 450 °C (from 250 °C); the absence of an increase in the TD-CRDS response verifies the absence of alkyl nitrates in the output of the photo source.

At 15:30, TD-CIMS and TD-CRDS sampled the output of the passive diffusion source containing a synthetic PPN standard. The two measurements are in quantitative agreement within the combined precisions of the two instruments. For example, at the highest mixing ratio, TD-CRDS measured (384 ± 40) pptv and TD-CIMS observed (364 ± 13) pptv. This confirms that calibrations utilizing the photochemical generation of PPN are accurate.

4. Discussion

4.1. Source photochemistry: ketone photolysis

The synthetic route used in this work is analogous to the generation of PAN from acetone photolysis. Photolysis of acetone in the formally spin-forbidden (n, π^*) band at around 280 nm results in C–C bond cleavage and produces alkyl and acyl radicals:

$$(R)_2CO + h\nu \rightarrow RCO^{\bullet} + R^{\bullet} \quad (1)$$

This process is known as a Norrish type 1 reaction and is well documented in text books on organic photochemistry. In the presence of O_2, the acyl radical is rapidly converted to the peroxyacyl radical which equilibrates (in the presence of NO_x) with the corresponding PAN.

$$RCO^{\bullet} + O_2 \rightarrow RC(O)O_2^{\bullet} \quad (2)$$

$$RC(O)O_2^{\bullet} + NO_2 \rightleftharpoons RC(O)O_2NO_2 \quad (3)$$

Since all simple ketones (with exception of aryl ketones) undergo Norrish type 1 reactions when irradiated in their (n, π^*) bands, it is not at all surprising that it is possible to generate peroxycarboxylic nitric anhydrides other than peroxyacetic nitric anhydride by this route. The (n, π^*) bands of other symmetric dialkyl ketones are only slightly red-shifted relative to that of acetone (Fig. 2; see also Chandler and Goodman, 1970; Hansen and Lee, 1975; Martinez et al., 1992; Yujing and Mellouki, 2000) such that the same photolysis source can be deployed to generate the other conjugate PANs. However, the PAN yields cannot be easily predicted, mainly since the photolysis quantum yields are only accurately known for acetone (e.g., (Blitz et al., 2004)). Our work

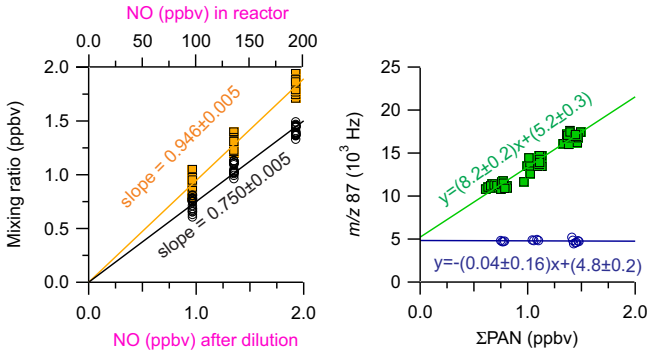

Fig. 7. Scatter plots of the PiBN data shown in Fig. 6, presented in the same way as in Fig. 5.

indicates that, at least for diethyl ketone and diisopropyl ketone, the quantum yields are high.

One of the key differences between photolysis of acetone, diethyl, and diisopropyl ketone is the nature of secondary products formed. For example, the acetone source is known to yield formaldehyde as a side product (e.g., (Ballesteros et al., 2007)). Likewise, photolysis of 3-pentanone yields acetaldehyde, which is a potential source of PAN. In other words, there exist chemical pathways for the smaller PANs to be generated in the PPN and PiBN sources, which would be quantified as part of ∑PAN by TD-CRDS, potentially presenting a systematic error. Monitoring the output of the PPN photo source by TD-CIMS, we observed up to 2000 counts of acetate and 48,200 counts of propanate in the CIMS mass spectrum, or 4% (Fig. 4). For the PiBN source, there were 300 counts at *m/z* 73 and 500 counts at *m/z* 59 for 17,000 counts at *m/z* 87, or 5%. These results indicate that formation of PAN side products via these channels is negligibly small.

4.2. Yield of PANs as a function of NO_x

Table 2 summarizes the yields of PAN, PPN, and PiBN as well as PAN + NO_2, PPN + NO_2, and PiBN + NO_2 as a function of NO (or NO_2) observed by TD-CRDS in several experiments. The uncertainties stated are the ±1 σ precisions of the slopes of the linear fits and do not include uncertainties in the calibration of the amount of NO (or NO_2) delivered; the scatter of the data in Table 2 suggests that this uncertainty can be quite large (in the range of 5–10%). Even though the source output scales linearly with the amount of NO_x added to the photo source, we do not use this relationship for calibration purposes. Instead, we rely on measurements of the source output by TD-CRDS, which is more accurate and does not depend on one's ability to deliver an accurately calibrated gas stream containing NO.

The data in Table 2 show similar yields when either NO_2 or NO are used as reagent, which implies that either can be used to generate PPN or PiBN in high yield. However, we prefer to use NO_2 as a reagent because the total amounts of PPN and PiBN generally appeared to be slightly larger and because oxidation of NO by PP (or PiB) radical produces radical species such as OH and alkyl peroxy radicals, which can lead to undesired side products. For example, alkyl peroxy and alkoxy radicals, generated via reactions (4–6),

$$RC(O)O_2^{\bullet} + NO \rightarrow RC(O)O^{\bullet} + NO_2 \rightarrow R^{\bullet} + CO_2 + NO_2 \quad (4)$$

$$R^{\bullet} + O_2 \rightarrow RO_2^{\bullet} \quad (5)$$

$$RO_2^{\bullet} + NO \rightarrow RO^{\bullet} + NO_2 \quad (6)$$

can react with NO_x to form alkyl nitrates (Shepson, 2007):

$$RO_2^{\bullet} + NO \rightarrow RO_2NO \rightarrow RONO_2 \quad (7)$$

$$RO^{\bullet} + NO_2 \rightarrow RONO_2 \quad (8)$$

The yields of alkyl nitrates are likely larger for radicals generated from diisopropyl ketone (due to their greater degree of substitution) than for the smaller diketones. Decomposition of the alkoxy radicals leads to formation of HO_x (=OH + HO_2) and, potentially, HNO_3, for example:

$$RCH_2O^{\bullet} + O_2 \rightarrow HO_2^{\bullet} + RCHO \quad (9)$$

$$HO_2^{\bullet} + NO \rightarrow OH^{\bullet} + NO_2 \quad (10)$$

$$OH^{\bullet} + NO_2 \rightarrow HNO_3 \quad (11)$$

Thus, the use of NO can promote formation of unfavorable side products. In previous work, NO was chosen primarily because its output from standard cylinders is more reliable and more easily calibrated than that of NO_2 containing cylinders; since we do not rely on a calibrated output of a NO_x reference gas in this study, we see no advantage in using NO as a reagent gas, and therefore choose to convert NO to NO_2 prior to entering the reaction chamber. Unlike earlier studies, the photochemistry, i.e., reaction (3) is not driven to completion with respect to NO_2, i.e., there is some unreacted NO_2 co-emitted by the source. Since we explicitly monitor NO_2 by TD-CRDS, there is no disadvantage as calibration of the TD-CIMS is still possible, yet this approach allows us to keep the photochemistry to a minimum and to minimize potential side reactions, including photolysis of the PAN photoproducts (Fig. 9).

4.3. Considerations in the calibration of TD-CIMS: accuracy and interferences

We observed noticeable offset counts at *m/z* 59 (not shown), *m/z* 73 (Fig. 5, rhs), and *m/z* 87 (Fig. 7, rhs) when the photo sources were used, These offsets were not titrated by NO and are therefore not due to PAN compounds. Furthermore, these offsets did not scale with the amount of NO_x added to the photo source. Their origin is not known with certainty; however, we speculate that the offset counts are due to peroxycarboxylic acids generated from reaction of PA, PP, or PiB radical with HO_2 in the photo source:

$$RC(O)O_2^{\bullet} + HO_2 \rightarrow RC(O)OOH + O_2 \quad (12)$$

The peroxycarboxylic acids are known to readily react with iodide ion in aqueous solution, and it is reasonable to assume that this reaction is also efficient in the gas-phase in the TD-CIMS inlet:

$$RC(O)OOH + I^- \rightarrow RC(O)O^- + HOI \quad (13)$$

Comparison of the slopes of the rhs plot in Fig. 5 with that obtained using a synthetic standard (data not shown) shows that the calibration using the photochemical generation of PPN is accurate. This is in contrast to the results obtained with PiBN (Table 3): The response factor of the scatter plot of *m/z* 87 against ∑PAN (Fig. 7, rhs) is 60% larger than that obtained using a synthetic standard for reasons that are unclear. The observed levels of NO_2+∑PAN are consistent with the amount of NO added to the photo source (Fig. 7, lhs) and with simultaneous measurements of

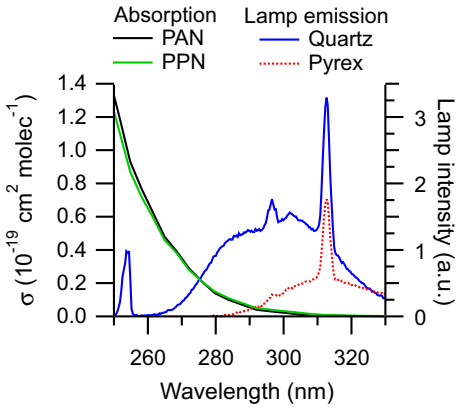

Fig. 9. Overlap of the PAN and PPN absorption spectra with the lamp emission spectra. The PAN and PPN spectra were obtained from the NASA–JPL evaluation (Sander et al., 2006) with data from Talukdar et al. (1995) and Harwood et al. (2003). There is significant overlap of PAN and PPN absorption with the lamp emission spectrum when the quartz cell is used, but not when the Pyrex cell is used.

NO_y, which corroborates that the TD-CRDS is accurately quantifying the amount of $\sum$PAN generated. The most plausible explanation, therefore, is that the TD-CIMS is converting an unidentified species co-emitted by the photo source to a species that is detected at *m/z* 87 and is titrated by NO.

4.4. Comparison to photo sources described in the literature

The results with the PPN photo source obtained in this study are an improvement on the work reported by Volz-Thomas et al. (2002) who attempted to synthesize PPN from photolysis of 3-pentanone in the presence of NO but reported significant formation of ethyl nitrate as a side product. While we did not have the chance to directly compare the output of the source described by Volz-Thomas et al. (2002) with ours, we believe that our results with the quartz source allows us to rationalize the difference in product ratios obtained. The quartz photolysis chamber in our laboratory was constructed following the description by Flocke et al. (2005) who modified a photolysis chamber supplied by Metcon (which is based on the design by Volz-Thomas et al. (2002)). Our results obtained with the quartz reactor are consistent with the results observed by Volz-Thomas et al. (2002), in that we show that alkyl nitrates are indeed formed in a quartz cell, but not when 254 nm light is suppressed through use of a Pyrex photo reactor. Suppression of 254 nm light likely suppresses formation of HO_x and photolysis of PANs (Fig. 9). Photolysis of PAN and PPN produces NO_3 with 40% quantum yield (Harwood et al., 2003), which potentially increases the yield of alkyl nitrates as the highly reactive NO_3 either reacts with PA radical (Harwood et al., 2003) or with alkyl peroxy radicals to form alkoxy radicals. Furthermore, the NO_3 produced has a high probability to convert to nitric acid, another undesired side product.

5. Conclusions and future work

The technique described here allows the generation of gas streams containing trace amounts of PAN, PPN, or PiBN at concentration levels comparable to those found in ambient air. Parallel measurements of the output of the photo source by TD-CRDS enabled accurate calibration of a TD-CIMS for PAN and PPN. The TD-CIMS exhibited a consistently 60% larger response to photochemically generated PiBN than for PiBN eluted from a diffusion source containing a synthetic standard, for reasons that are not well understood.

Acknowledgments

This work was financially supported by an Alberta Ingenuity New Faculty Award, the National Science and Engineering Research Council of Canada (NSERC) in the form of Discovery and Research Tools and Instruments (RTI) grants, and the University of Calgary via startup funds. Amanda Furgeson was supported by an NSERC Alexander Graham Bell Scholarship.

References

Ballesteros, B., Garzon, A., Jimenez, E., Notario, A., Albaladejo, J., 2007. Relative and absolute kinetic studies of 2-butanol and related alcohols with tropospheric Cl atoms. Physical Chemistry Chemical Physics 9, 1210–1218.

Blitz, M.A., Heard, D.E., Pilling, M.J., Arnold, S.R., Chipperfield, M.P., 2004. Pressure and temperature-dependent quantum yields for the photodissociation of acetone between 279 and 327.5 nm. Geophysical Research Letters 31, L06111.

Chandler, W.D., Goodman, L., 1970. Allowed and forbidden character in the $[\pi]^* \leq n$ band in symmetric alkyl ketones. Journal of Molecular Spectroscopy 36, 141–154.

Darley, E.F., Kettner, K.A., Stephens, E.R., 1963. Analysis of peroxyacyl nitrates by gas chromatography with electron capture detection. Analytical Chemistry 35, 589–591.

Emrich, M., Warneck, P., 2000. Photodissociation of acetone in air: dependence on pressure and wavelength. Behavior of the excited singlet state. Journal of Physical Chemistry A 104, 9436–9442.

Flocke, F.M., Weinheimer, A.J., Swanson, A.L., Roberts, J.M., Schmitt, R., Shertz, S., 2005. On the measurement of PANs by gas chromatography and electron capture detection. Journal of Atmospheric Chemistry 52, 19–43.

Gaffney, J.S., Fajer, R., Senum, G.I., 1984. An improved procedure for high-purity gaseous peroxyacyl nitrate production – use of heavy lipid solvents. Atmospheric Environment 18, 215–218.

Grosjean, D., Fung, K., Collins, J., Harrison, J., Breitung, E., 1984. Portable generator for on-site calibration of peroxyacetyl nitrate analyzers. Analytical Chemistry 56, 569–573.

Hansen, D.A., Lee, E.K.C., 1975. Radiative and nonradiative transitions in the first excited singlet state of symmetrical methyl-substituted acetones. The Journal of Chemical Physics 62, 183–189.

Harwood, M.H., Roberts, J.M., Frost, G.J., Ravishankara, A.R., Burkholder, J.B., 2003. Photochemical studies of $CH_3C(O)OONO_2$ (PAN) and $CH_3CH_2C(O)OONO_2$ (PPN): NO_3 quantum yields. Journal of Physical Chemistry A 107, 1148–1154.

Martinez, R.D., Buitrago, A.A., Howell, N.W., Hearn, C.H., Joens, J.A., 1992. The near-UV absorption spectra of several aliphatic aldehydes and ketones at 300 K. Atmospheric Environment Part A – General Topics 26, 785–792.

Nielsen, T., Hansen, A.M., Thomsen, E.L., 1982. A convenient method for preparation of pure standards of peroxyacetyl nitrate for atmospheric analyses. Atmospheric Environment 16, 2447–2450.

Pätz, H.-W., Lerner, A., Houben, N., Volz-Thomas, A., 2002. Validation of a new method for the calibration of peroxy acetyl nitrate (PAN)-analyzers. Gefahrstoffe Reinhaltung der Luft 62, 215–219.

Paul, D., Furgeson, A., Osthoff, H.D., 2009. Measurement of total alkyl and peroxy nitrates by thermal decomposition cavity ring-down spectroscopy. Review of Scientific Instruments 80, 114101. doi:114110.111063/114101.3258204.

Paul, D., Osthoff, H.D., 2010. Absolute measurements of total peroxy nitrate mixing ratios by thermal dissociation blue diode laser cavity ring-down spectroscopy. Analytical Chemistry 82, 6695–6703.

Roberts, J.M., 1990. The atmospheric chemistry of organic nitrates. Atmospheric Environment Part A – General Topics 24, 243–287.

Roberts, J.M., 2007. PAN and related Compounds. In: Koppmann, R. (Ed.), Volatile Organic Compounds in the Atmosphere. Blackwell Publishing, Oxford, UK, pp. 221–268.

Sander, S.P., Friedl, R.R., Ravishankara, A.R., Golden, D.M., Kolb, C.E., Kurylo, M.J., Molina, M.J., Moortgat, G.K., Keller-Rudek, H., Finlayson-Pitts, B.J., Wine, P.H., Huie, R.E., Orkin, V.L., 2006. Chemical Kinetics and Photochemical Data for Use in Atmospheric Studies, Evaluation Number 15. NASA/JPL, Pasadena, CA.

Schrimpf, W., Müller, K.P., Johnen, F.J., Lienaerts, K., Rudolph, J., 1995. An optimized method for airborne peroxyacetyl nitrate (PAN) measurements. Journal of Atmospheric Chemistry 22, 303–317.

Shepson, P.B., 2007. Organic nitrates. In: Koppmann, R. (Ed.), Volatile Organic Compounds in the Atmosphere, pp. 269–291.

Slusher, D.L., Huey, L.G., Tanner, D.J., Flocke, F.M., Roberts, J.M., 2004. A thermal dissociation-chemical ionization mass spectrometry (TD-CIMS) technique for the simultaneous measurement of peroxyacyl nitrates and dinitrogen pentoxide. Journal of Geophysical Research-Atmospheres 109, D19315. doi:19310.11029/12004JD004670.

Talukdar, R.K., Burkholder, J.B., Schmoltner, A.M., Roberts, J.M., Wilson, R.R., Ravishankara, A.R., 1995. Investigation of the loss processess for peroxyacetyl nitrate in the atmosphere – UV Photolysis and reaction with OH. Journal of Geophysical Research-Atmospheres 100, 14163–14173.

Volz-Thomas, A., Xueref, I., Schmitt, R., 2002. An automatic gas chromatograph 426 and calibration system for ambient measurements of PAN and PPN. Environmental Science and Pollution Research 9, 72–76.

Warneck, P., Zerbach, T., 1992. Synthesis of peroxyacetyl nitrate in air by acetone photolysis. Environment Science and Technology 26, 74–79.

Williams, J., Roberts, J.M., Bertman, S.B., Stroud, C.A., Fehsenfeld, F.C., Baumann, K., Buhr, M.P., Knapp, K., Murphy, P.C., Nowick, M., Williams, E.J., 2000. A method for the airborne measurement of PAN, PPN, and MPAN. Journal of Geophysical Research-Atmospheres 105, 28943–28960.

Yujing, M., Mellouki, A., 2000. The near-UV absorption cross sections for several ketones. Journal of Photochemistry and Photobiology A: Chemistry 134, 31–36.

Zheng, W., Flocke, F.M., Tyndall, G.S., Swanson, A., Orlando, J.J., Roberts, J.M., Huey, L.G., Tanner, D.J., 2011. Characterization of a thermal decomposition chemical ionization mass spectrometer for the measurement of peroxy acyl nitrates (PANs) in the atmosphere. Atmospheric Chemistry and Physics Discussion 11, 8461–8513.